

**CHARACTERIZATION, KINETICS AND
EQUILIBRIUM STUDIES OF PARACETAMOL
ADSORPTION ON THE OIL PALM FRONDS
(OPF) CELLULOSE NANOCRYSTALS**

NOR NAJHAN BINTI IDRIS

UNIVERSITI SAINS MALAYSIA

2022

**CHARACTERIZATION, KINETICS AND
EQUILIBRIUM STUDIES OF PARACETAMOL
ADSORPTION ON THE OIL PALM FRONDS
(OPF) CELLULOSE NANOCRYSTALS**

by

NOR NAJHAN BINTI IDRIS

**Thesis submitted in fulfilment of the requirements
for the degree of
Master of Science**

February 2022

ACKNOWLEDGEMENT

First and foremost, I wish to express my gratitude to Allah SWT for giving me an opportunity and good health during the completion and chance to write this project. My first appreciation goes to my supervisor, Professor Madya Dr. Mohd Hazwan Hussin from Universiti Sains Malaysia, and my field supervisors, Dr. Lisman Suryanegara (Indonesian Institute of Science, LIPI) and Mrs. Nor Salmi Abdullah (National Hydraulic Research Institute of Malaysia, NAHRIM) for their invaluable continuous support, guidance, patience, and advice throughout my undertaking of this research project. I must express my profound thanks to the Research University Incentive, RUI grant (1001/PKIMIA/8011077), and USM External Grant (304/PKIMIA/6501094/I129). I am also pleased to acknowledge all the administrative and technical staff, especially the science officers and laboratory assistants at the School of Chemical Sciences, the School of Biology, the School of Physics, the School of Industrial Technology, and the Archaeology Research Centre USM, who had helped me throughout my research. Most importantly, very special gratitude goes out to all my family members, especially my late father, Idris Hussin, my mother, Wan Faridah Wan Awang, and my siblings, for their endless prayers, financial and moral support, and determination to educate me to complete this thesis. Finally, my special thanks to my fellow lab mates and friends, especially Farah, Shafiqah, Alif, Sherwyn, Rushan, Fatin, Kak Hanis, and Kak Hidayah, for their time in guiding and helping me during my research work. Thank you so much.

TABLE OF CONTENTS

ACKNOWLEDGEMENT	ii
TABLE OF CONTENTS	iii
LIST OF TABLES	viii
LIST OF FIGURES	x
LIST OF SYMBOLS	xv
LIST OF ABBREVIATIONS	xviii
LIST OF APPENDICES	xx
ABSTRAK	xxi
ABSTRACT	xxiii
CHAPTER 1 INTRODUCTION	1
1.1 Background study	1
1.2 Problem statement	3
1.3 Research objectives	5
1.4 Scope of study	5
CHAPTER 2 LITERATURE REVIEW	6
2.1 Oil palm (<i>Elaeis guineensis</i>)	6
2.2 Combinative pre-treatment process	8
2.2.1 Autohydrolysis	9
2.2.2 Delignification process	11
2.2.2(a) Soda pulping	11
2.3 Chemical techniques for CNC isolation	12
2.3.1 Acid hydrolysis	14
2.3.1(a) Cellulose hydrolytic mechanism in acid hydrolysis	17
2.4 Cellulose	21
2.5 Cellulose nanocrystals (CNC)	25

2.6	Cellulose-based adsorbents	28
2.7	Pharmaceuticals in wastewater.....	32
2.8	Technologies for pharmaceutical removal	35
2.9	Adsorption process	38
2.9.1	Adsorption isotherms.....	41
2.9.1(a)	Langmuir isotherm.....	41
2.9.1(b)	Freundlich isotherm.....	43
2.9.1(c)	Temkin isotherm.....	44
2.9.1(d)	Dubinin-Radushkevich isotherm	44
2.9.2	Adsorption kinetics	45
2.9.2(a)	Pseudo-first order model.....	46
2.9.2(b)	Pseudo-second order model.....	46
2.9.2(c)	Elovich kinetic model	47
2.9.2(d)	Intra-particle diffusion model.....	48
CHAPTER 3 MATERIALS AND METHODS.....		49
3.1	Chemicals and reagents	49
3.2	Sample preparation.....	51
3.3	Autohydrolysis process	51
3.4	Soda pulping.....	51
3.5	Pulp bleaching	52
3.6	Mercerization	52
3.7	Acid hydrolysis	53
3.8	Characterisation of cellulose nanocrystals (CNC)	53
3.8.1	Fourier transform infrared spectroscopy (FTIR) analysis	54
3.8.2	Solid-state ¹³ C cross-polarization/magic angle spinning nuclear magnetic resonance (CP/MAS ¹³ C NMR) analysis.....	54
3.8.3	X-Ray Diffraction (XRD) analysis.....	54
3.8.4	Thermal behaviour.....	55

3.8.5	Surface and morphology analyses	55
3.9	Preparation of OPF CNC hydrogel beads	56
3.9.1	Preparation of stock solution	57
3.9.2	Adsorption experiments.....	57
3.9.2(a)	Effect of adsorbent dosage.....	58
3.9.2(b)	Point of zero charge (pH_{pzc}) and effect of pH	58
3.9.2(c)	Effect of contact time.....	59
3.9.2(d)	Effect of paracetamol concentration.....	59
3.10	Characterisation of OPF CNC hydrogel beads	60
3.10.1	FTIR, BET, SEM, and EDX analyses	60
3.11	Preparation of OPF CNC-AC hydrogel beads	60
3.11.1	Adsorption experiments.....	61
3.11.1(a)	Effect of pH	61
3.11.1(b)	Effect of contact time	61
3.11.1(c)	Effect of paracetamol concentration.....	61
3.12	Characterisation of OPF CNC-AC hydrogel beads.....	61
3.12.1	FTIR, BET, SEM, EDX and XPS analyses.....	61
3.13	Reusability of OPF CNC and OPF CNC-AC hydrogel beads	62
CHAPTER 4 RESULTS AND DISCUSSION.....		63
4.1	Cellulosic yields	63
4.2	Characterisation of OPF CNC.....	64
4.2.1	FTIR analysis.....	64
4.2.2	CP/MAS ^{13}C NMR analysis	67
4.2.3	XRD analysis.....	69
4.2.4	Thermal analyses	72
4.2.4(a)	Thermogravimetric analysis (TGA)	72
4.2.4(b)	Differential scanning calorimetry (DSC)	76

4.2.5	Surface and morphology analyses.....	77
4.2.5(a)	BET analysis.....	77
4.2.5(b)	SEM.....	80
4.2.5(c)	TEM.....	81
4.3	Adsorption studies of OPF CNC hydrogel beads.....	83
4.3.1	Effect of adsorbent dosage	83
4.3.2	Point of zero charge (pH_{pzc}) and effect of pH	85
4.3.3	Effect of contact time	88
4.3.4	Effect of paracetamol concentration.....	90
4.4	Adsorption isotherms of OPF CNC hydrogel beads	92
4.4.1	Langmuir isotherm	93
4.4.2	Freundlich isotherm.....	95
4.4.3	Temkin isotherm.....	98
4.4.4	Dubinin-Raduskevich isotherm	99
4.5	Adsorption kinetics of OPF CNC hydrogel beads	101
4.5.1	Pseudo-first order	101
4.5.2	Pseudo-second order.....	103
4.5.3	Elovich kinetic model.....	105
4.5.4	Intra-particle diffusion.....	106
4.6	Paracetamol adsorption mechanism by OPF CNC hydrogel beads	109
4.7	Characterisation of OPF CNC hydrogel beads	111
4.7.1	FTIR	111
4.7.2	BET.....	113
4.7.3	SEM and EDX.....	114
4.8	Adsorption studies of OPF CNC-AC hydrogel beads.....	119
4.8.1	Effect of pH.....	119
4.8.2	Effect of contact time	121

4.8.3	Effect of initial paracetamol concentration	123
4.9	Adsorption isotherms of OPF CNC-AC hydrogel beads	125
4.9.1	Langmuir isotherm	125
4.9.2	Freundlich isotherm.....	129
4.9.3	Temkin isotherm.....	131
4.9.4	Dubinin-Raduskevich isotherm	132
4.10	Adsorption kinetics OPF CNC-AC hydrogel beads.....	133
4.10.1	Pseudo-first order	133
4.10.2	Pseudo-second order.....	135
4.10.3	Elovich kinetic model.....	136
4.10.4	Intra-particle diffusion.....	138
4.11	Paracetamol adsorption mechanism by OPF CNC-AC hydrogel beads	140
4.12	Characterisation of OPF CNC-AC hydrogel beads.....	142
4.12.1	FTIR	142
4.12.2	BET.....	144
4.12.3	SEM and EDX.....	146
4.12.4	XPS.....	149
4.13	Reusability of OPF CNC and OPF CNC-AC hydrogel beads	150
CHAPTER 5 CONCLUSION AND FUTURE RECOMMENDATIONS		154
5.1	Conclusion.....	154
5.2	Recommendations for future research.....	156
REFERENCES.....		158
APPENDICES		
LIST OF PUBLICATIONS AND EXHIBITION		

LIST OF TABLES

	Page
Table 2. 1	Oil palm planted area by state in December 2020 (MPOB)7
Table 2. 2	Different types of acid used to form cellulose derivatives from various kinds of sources and their crystallinity index 17
Table 2. 3	CNC extraction from various parts of oil palm biomass and their properties.....27
Table 2. 4	Comparison of adsorption efficiency and cellulose-based adsorbent from different sources in the adsorption of various pollutants31
Table 2. 5	Adsorption studies of paracetamol from different types of adsorbents and their maximum adsorption capacities.....37
Table 2. 6	Linear forms of Langmuir isotherms42
Table 4. 1	FTIR spectral peak assignments for α -cellulose and OPF CNC65
Table 4. 2	Crystallinity index for α -cellulose and OPF CNC 72
Table 4. 3	Thermal properties of α -cellulose and OPF CNC 74
Table 4. 4	Surface and porosity parameters of grounded OPF and OPF CNC obtained from BET analysis..... 78
Table 4. 5	Langmuir parameters of OPF CNC hydrogel beads by linear regression method95
Table 4. 6	Isotherm parameters values of paracetamol adsorption on OPF CNC hydrogel beads at pH 3, 60 g of dosage and temperature of $(27 \pm 1 \text{ }^\circ\text{C})$97
Table 4. 7	The pseudo-first order kinetic model for adsorption of paracetamol on OPF CNC hydrogel beads adsorbent 103
Table 4. 8	The pseudo-second order kinetic model for adsorption of paracetamol on OPF CNC hydrogel beads adsorbent..... 105

Table 4. 9	The Elovich kinetic model for adsorption of paracetamol on OPF CNC hydrogel beads adsorbent.....	106
Table 4. 10	The intra-particle diffusion constant and linear regression coefficients at 10 mg L ⁻¹ paracetamol concentration	109
Table 4. 11	Surface and porosity parameters of alginate hydrogel beads and OPF CNC hydrogel beads obtained from BET analysis.....	114
Table 4. 12	Elemental weight for alginate hydrogel beads and OPF CNC hydrogel beads before and after adsorption	116
Table 4. 13	Langmuir parameters of OPF CNC-AC hydrogel beads by linear regression method	126
Table 4. 14	Comparison of monolayer adsorption capacities of paracetamol on different adsorbents	128
Table 4. 15	Isotherm parameters values of paracetamol adsorption onto OPF CNC-AC hydrogel beads at (27 ± 1 °C)	130
Table 4. 16	The pseudo-first order kinetic model for adsorption of paracetamol on OPF CNC-AC hydrogel beads adsorbent	135
Table 4. 17	The pseudo-second order kinetic model for adsorption of paracetamol on OPF CNC-AC hydrogel beads adsorbent.....	136
Table 4. 18	The Elovich kinetic model for adsorption of paracetamol on OPF CNC-AC hydrogel beads adsorbent.....	138
Table 4. 19	The intra-particle diffusion constant and linear regression coefficients at 10 mg L ⁻¹ paracetamol concentration	140
Table 4. 20	Surface and porosity parameters of commercial activated carbon and OPF CNC-AC hydrogel beads obtained from BET analysis	145
Table 4. 21	Elemental weight for OPF CNC-AC hydrogel beads before and after adsorption.....	147

LIST OF FIGURES

	Page
Figure 2. 1	Schematic diagram of pre-treatment on lignocellulosic biomass9
Figure 2. 2	A possible mechanism during autohydrolysis process..... 10
Figure 2. 3	Mechanism of lignin during soda pulping process 12
Figure 2. 4	(a) Schematic diagram of the amorphous and crystalline regions in cellulose break down during acid hydrolysis and (b) isolated CNC 15
Figure 2. 5	The acid formation in cellulose..... 19
Figure 2. 6	Mechanism of acid hydrolysis of glycosidic bonds 20
Figure 2. 7	Molecular structure of cellulose chain where n is the value of a degree of polymerization..... 22
Figure 2. 8	Structure of cellulose I (a) and cellulose II (b) 24
Figure 2. 9	Chemical structure of paracetamol..... 35
Figure 2. 10	Diagrammatic representation of isotherm classifications 40
Figure 3. 1	The research workflow 50
Figure 4. 1	The chemical structure of cellulose and FTIR spectra of (a) α -cellulose and (b) OPF CNC 65
Figure 4. 2	The CP/MAS ¹³ C NMR spectra of (A) α -cellulose and (B) OPF CNC 68
Figure 4. 3	X-ray diffractograms of (a) OPF CNC and (b) α -cellulose 70
Figure 4. 4	TGA (a) and DTG (b) thermograms of α -cellulose and OPF CNC... 75
Figure 4. 5	DSC thermograms of α -cellulose and OPF CNC 77
Figure 4. 6	N ₂ adsorption-desorption isotherm plots for (a) raw OPF and (b) OPF CNC 79
Figure 4. 7	SEM micrographs of (a) α -cellulose and (b) OPF CNC at 1000x magnification..... 80

Figure 4. 8	TEM image of OPF CNC at 31500x magnification.....	82
Figure 4. 9	Percentage removal and adsorption capacity of paracetamol with OPF CNC hydrogel beads at pH 5.8 and temperature of $(27 \pm 1 \text{ }^\circ\text{C})$	84
Figure 4. 10	pH_{pzc} of OPF CNC hydrogel beads at dosage of 60 g and temperature of $(27 \pm 1 \text{ }^\circ\text{C})$	86
Figure 4. 11	Percentage removal and effect of pH on paracetamol with OPF CNC hydrogel beads dosage at 60 g and temperature of $(27 \pm 1 \text{ }^\circ\text{C})$	87
Figure 4. 12	Percentage removal and effect of contact time on paracetamol by OPF CNC hydrogel beads at pH 3, 60 g dosage and temperature of $(27 \pm 1 \text{ }^\circ\text{C})$	89
Figure 4. 13	Percentage removal and effect of initial paracetamol concentration by OPF CNC hydrogel beads at pH 3, 60 g dosage, and temperature of $(27 \pm 1 \text{ }^\circ\text{C})$ for 170 min	91
Figure 4. 14	Langmuir-2 isotherm plot of paracetamol adsorption on OPF CNC hydrogel beads at pH 3, 60 g dosage and temperature of $(27 \pm 1 \text{ }^\circ\text{C})$	94
Figure 4. 15	Freundlich isotherm plot of paracetamol adsorption on OPF CNC hydrogel beads at pH 3, 60 g dosage and temperature of $(27 \pm 1 \text{ }^\circ\text{C})$	97
Figure 4. 16	Temkin isotherm plot of paracetamol adsorption on OPF CNC hydrogel beads at pH 3, 60 g dosage and temperature of $(27 \pm 1 \text{ }^\circ\text{C})$	99
Figure 4. 17	Dubinin-Radushkevich isotherm plot of paracetamol adsorption on OPF CNC hydrogel beads at pH 3, 60 g dosage and temperature of $(27 \pm 1 \text{ }^\circ\text{C})$	100
Figure 4. 18	Pseudo-first order kinetic model plot for the adsorption of paracetamol on OPF CNC hydrogel beads at pH 3, 60 g of dosage and temperature of $(27 \pm 1 \text{ }^\circ\text{C})$	102

Figure 4. 19	Pseudo-second order kinetic model plot for the adsorption of paracetamol on OPF CNC hydrogel beads at pH 3, 60 g of dosage and temperature of $(27 \pm 1 \text{ }^\circ\text{C})$	104
Figure 4. 20	Elovich kinetic model plot for the adsorption of paracetamol on OPF CNC hydrogel beads at pH 3, 60 g of dosage and temperature of $(27 \pm 1 \text{ }^\circ\text{C})$	106
Figure 4. 21	Intra-particle diffusion model plot for the adsorption of paracetamol on OPF CNC hydrogel beads at pH 3, 60 g of dosage and temperature of $(27 \pm 1 \text{ }^\circ\text{C})$	108
Figure 4. 22	Schematic illustration of paracetamol adsorption onto OPF CNC hydrogel beads	111
Figure 4. 23	FTIR spectra of (a) OPF CNC hydrogel beads before adsorption, (b) paracetamol, and (c) OPF CNC hydrogel beads after adsorption	112
Figure 4. 24	SEM images of (a) cross-section of alginate hydrogel bead, (b) and (d) surface morphology of OPF CNC hydrogel beads (before and after adsorption), (c) and (e) cross-section of OPF CNC hydrogel beads (before and after adsorption) at 200 \times magnification	115
Figure 4. 25	EDX spectra of (a) alginate hydrogel beads, (b) OPF CNC hydrogel beads (before adsorption), and (c) OPF CNC hydrogel beads (after adsorption).....	118
Figure 4. 26	Percentage removal and effect of pH on paracetamol with OPF CNC-AC hydrogel beads dosage at 0.6 g and temperature of $(27 \pm 1 \text{ }^\circ\text{C})$	120
Figure 4. 27	Percentage removal and effect of contact time on paracetamol by OPF CNC-AC hydrogel beads at pH 3, 0.6 g dosage and temperature of $(27 \pm 1 \text{ }^\circ\text{C})$	122
Figure 4. 28	Percentage removal and effect of initial paracetamol concentration by OPF CNC-AC hydrogel beads at pH 3, 0.6 g dosage and temperature of $(27 \pm 1 \text{ }^\circ\text{C})$ for 170 min	124

Figure 4. 29	Langmuir-1 isotherm plot of paracetamol adsorption on OPF CNC-AC hydrogel beads at pH 3, 0.6 g dosage and temperature of $(27 \pm 1 \text{ }^\circ\text{C})$	125
Figure 4. 30	Freundlich isotherm plot of paracetamol adsorption on OPF CNC-AC hydrogel beads at pH 3, 0.6 g dosage and temperature of $(27 \pm 1 \text{ }^\circ\text{C})$	130
Figure 4. 31	Temkin isotherm plot of paracetamol adsorption on OPF CNC-AC hydrogel beads at pH 3, 0.6 g dosage and temperature of $(27 \pm 1 \text{ }^\circ\text{C})$	131
Figure 4. 32	Dubinin-Radushkevich isotherm plot of paracetamol adsorption on OPF CNC-AC hydrogel beads at pH 3, 0.6 g dosage and temperature of $(27 \pm 1 \text{ }^\circ\text{C})$	133
Figure 4. 33	Pseudo-first order kinetic model plot for the adsorption of paracetamol on OPF CNC-AC hydrogel beads at pH 3, 0.6 g of dosage and temperature of $(27 \pm 1 \text{ }^\circ\text{C})$	134
Figure 4. 34	Pseudo-second order kinetic model plot for the adsorption of paracetamol on OPF CNC-AC hydrogel beads at pH 3, 0.6 g of dosage and temperature of $(27 \pm 1 \text{ }^\circ\text{C})$	136
Figure 4. 35	Elovich kinetic model plot for the adsorption of paracetamol on OPF CNC-AC hydrogel beads at pH 3, 0.6 g of dosage and temperature of $(27 \pm 1 \text{ }^\circ\text{C})$	137
Figure 4. 36	Intra-particle diffusion model plot for the adsorption of paracetamol on OPF CNC-AC hydrogel beads at pH 3, 0.6 g of dosage and temperature of $(27 \pm 1 \text{ }^\circ\text{C})$	139
Figure 4. 37	Schematic illustration of paracetamol adsorption onto OPF CNC-AC hydrogel beads	142
Figure 4. 38	FTIR spectra of (a) OPF CNC-AC hydrogel beads before adsorption, (b) paracetamol, and (c) OPF CNC-AC hydrogel beads after adsorption.....	143
Figure 4. 39	SEM images of (a) and (c) surface morphology of OPF CNC-AC hydrogel beads (before and after adsorption), (b) and (d) cross-	

	section of OPF CNC-AC hydrogel beads (before and after adsorption) at 200× magnification	146
Figure 4. 40	EDX spectra of (a) OPF CNC-AC hydrogel beads (before adsorption) and (b) OPF CNC-AC hydrogel beads (after adsorption)	148
Figure 4. 41	XPS spectra of (a) OPF CNC-AC hydrogel beads (before adsorption) and (b) OPF CNC-AC hydrogel beads (after adsorption)	149
Figure 4. 42	Reusability cycles of (a) OPF CNC hydrogel beads and (b) OPF CNC-AC hydrogel beads	153

LIST OF SYMBOLS

%	Percentage
°C	Degree of Celcius
ΔG°	Gibbs free energy change (kJ mol^{-1})
ΔH_T	Heat adsorption (kJ mol^{-1})
β	Constant related to adsorption energy ($\text{mol}^2 \text{kJ}^{-2}$)
μm	Micrometre
B_T	Temkin isotherm constant associated with adsorbent-adsorbate interaction (L mg^{-1})
C_e	Equilibrium concentration (mg L^{-1})
cm	Centimetre
C_o	Initial concentration (mg L^{-1})
E_a	Mean adsorption energy (kJ mol^{-1})
g	Gram
g cm^{-1}	Gram per centimetre
h	Hour
Hz	Hertz
K	Kelvin
k_1	Pseudo-first order rate constant
k_2	Pseudo-second order rate constant
K_F	Freundlich constant related to maximum adsorption capacity (mg g^{-1})
kHz	Kilo hertz
kJ mol^{-1}	Kilo joule per mole
K_L	Langmuir adsorption constant (L mg^{-1})
K_p	Intra-particle diffusion rate constant ($\text{mg g}^{-1} \text{min}^{1/2}$)
K_T	Temkin isotherm equilibrium binding constant

kV	Kilo volt
L	Litre
L mg ⁻¹	Litre per milligram
m	Weight (g)
M	Molar
mg	Milligram
mg g ⁻¹	Milligram per gram
mg L ⁻¹	Milligram per litre
MHz	Mega hertz
min	Minute
mL	Millilitre
mL min ⁻¹	Millilitre per minute
M _n	Number average molecular weight
M _w	Weight average molecular weight
n	Freundlich constant related to maximum adsorption intensity (mg g ⁻¹)
nm	Nanometre
pH _f	Final pH
pH _i	Initial pH
pH _{pzc}	pH point of zero charge
q _e	Adsorption capacity at equilibrium (mg g ⁻¹)
q _{e,cal}	Calculated adsorption capacity at equilibrium (mg g ⁻¹)
q _{e,exp}	Experimental adsorption capacity at equilibrium (mg g ⁻¹)
q _{max}	Maximum adsorption capacity (mg g ⁻¹)
q _t	Adsorption capacity at time (mg g ⁻¹)
R	Gas constant (8.314 J mol ⁻¹ K ⁻¹)
R ²	Correlation coefficient
R _L	Dimensionless factor (from Langmuir)

t	Time (min)
T	Temperature (K)
T _m	Melting temperature
V	Volume (L)
W	Weight (g)
w/v	Weight per volume

LIST OF ABBREVIATIONS

AC	Activated carbon
BET	Brunauer-Emmett-Teller
MCC	Microcrystalline cellulose
CNC	Cellulose nanocrystals
CNF	Cellulose nanofibres
CNW	Cellulose nanowhiskers
CP/MAS	Cross-Polarization/Magic Angle Spinning
CrI	Crystallinity index
DP	Degree of polymerization
DSC	Differential Scanning Calorimetry
DTG	Derivatives thermograms
EDX	Energy Dispersive X-ray
EFB	Empty fruit bunches
FTIR	Fourier Transform Infrared Analysis
MF	Mesocarp fibre
NMR	Nuclear Magnetic Resonance
OPF	Oil palm frond
OPL	Oil palm leaves
OPT	Oil palm trunk
PKS	Palm kernel shell
ppm	Parts per million
rpm	Revolutions per minute
SEM	Scanning Electron Microscope
TEM	Transmission Electron Microscopy

TGA	Thermogravimetric Analysis
XPS	X-ray photoelectron spectroscopy
XRD	X-Ray Diffraction

LIST OF APPENDICES

Appendix A	UV-Vis spectrum of paracetamol
Appendix B	Calibration curve for paracetamol solution (2 – 10 mg L ⁻¹)
Appendix C	Calibration curve for paracetamol solution (1 – 1000 mg L ⁻¹)
Appendix D	Langmuir-1 isotherm plot of paracetamol adsorption on OPF CNC hydrogel beads at pH 3, 60 g dosage and temperature of (27 ± 1 °C)
Appendix E	Langmuir-3 isotherm plot of paracetamol adsorption on OPF CNC hydrogel beads at pH 3, 60 g dosage and temperature of (27 ± 1 °C)
Appendix F	Langmuir-4 isotherm plot of paracetamol adsorption on OPF CNC hydrogel beads at pH 3, 60 g dosage and temperature of (27 ± 1 °C)
Appendix G	Langmuir-2 isotherm plot of paracetamol adsorption on OPF CNC-AC hydrogel beads at pH 3, 0.6 g dosage and temperature of (27 ± 1 °C)
Appendix H	Langmuir-3 isotherm plot of paracetamol adsorption on OPF CNC-AC hydrogel beads at pH 3, 0.6 g dosage and temperature of (27 ± 1 °C)
Appendix I	Langmuir-4 isotherm plot of paracetamol adsorption on OPF CNC-AC hydrogel beads at pH 3, 0.6 g dosage and temperature of (27 ± 1 °C)
Appendix J	Calculation of Gibbs free energy (ΔG°) for the adsorption of paracetamol onto OPF CNC hydrogel beads
Appendix K	Calculation of Gibbs free energy (ΔG°) for the adsorption of paracetamol onto OPF CNC-AC hydrogel beads

**PENCIRIAN, KAJIAN KINETIK DAN KESEIMBANGAN
PENJERAPAN PARASETAMOL PADA SELULOSA NANOKRISTAL
PELEPAH KELAPA SAWIT**

ABSTRAK

Pencemaran air akibat ubat-ubatan farmaseutikal contohnya parasetamol telah menjadi isu yang sangat membimbangkan; dan langkah-langkah berkesan harus diambil untuk merawat pencemaran air ini. Oleh itu, kajian ini meneroka penggunaan selulosa nanokristal (CNC) yang diasingkan dari pelepah kelapa sawit (OPF) melalui pra-rawatan dan hidrolisis asid sebagai penjerap. Analisis pelengkap menunjukkan bahawa OPF CNC memiliki indeks penghabluran 43.60 %, luas permukaan sebanyak $10.51 \text{ m}^2 \text{ g}^{-1}$, dan nisbah aspek 19.98. Selain itu, manik hidrogel OPF CNC dan OPF CNC-AC telah berjaya dihasilkan, dioptimumkan, dan digunakan untuk penyingkiran parasetamol. Pengubahsuaian manik hidrogel OPF CNC-AC dengan karbon aktif komersial (AC) telah meningkatkan luas permukaan BET sehingga $85.19 \text{ m}^2 \text{ g}^{-1}$. Kajian penjerapan parasetamol pada manik hidrogel OPF CNC dan OPF CNC-AC dapat dicapai masing-masing pada 60 g dan 0.6 g dos penjerap, pada nilai pH 3 dengan masa sentuhan 170 min pada suhu bilik. Kajian mendapati bahawa data yang diperoleh bertepatan dengan model kinetik pseudo-kedua dan model isoterma Freundlich bagi mencirikan penjerapan parasetamol pada manik hidrogel OPF CNC dengan kapasiti penjerapan maksimum, $q_{\max} 0.03 \text{ mg g}^{-1}$. Sementara itu, untuk manik hidrogel OPF CNC-AC, model kinetik pseudo-kedua dan model isoterma Langmuir menunjukkan hubungan terbaik bagi penjerapan parasetamol dengan nilai $q_{\max} 21.31 \text{ mg g}^{-1}$. Oleh itu, hasil dari kajian ini menunjukkan bahawa manik hidrogel OPF CNC dan OPF

CNC-AC dapat digunakan sebagai penjerap semula jadi untuk membuang sisa parasetamol.

**CHARACTERIZATION, KINETICS AND EQUILIBRIUM STUDIES
OF PARACETAMOL ADSORPTION ON THE OIL PALM FRONDS (OPF)
CELLULOSE NANOCRYSTALS**

ABSTRACT

Pollution of water *via* pharmaceutical drugs such as paracetamol have been a highly concerning issue; and effective measures must be taken to treat these aquatic contaminants. Hence, the present study explored use of cellulose nanocrystals (CNC) isolated from oil palm fronds (OPF) through pre-treatments and acid hydrolysis as an environmental friendly adsorbent. The complementary analyses showed that the OPF CNC possesses a crystallinity index of 43.60 %, surface area ($10.51 \text{ m}^2 \text{ g}^{-1}$), and an aspect ratio of 19.98. Besides, the OPF CNC and OPF CNC-AC hydrogel beads have been successfully produced, optimised, and applied for paracetamol removal. The modification of OPF CNC-AC hydrogel beads with the commercial activated carbon (AC) has improved the BET surface area up to $85.19 \text{ m}^2 \text{ g}^{-1}$. The adsorption studies of paracetamol onto OPF CNC and OPF CNC-AC hydrogel beads can be achieved at 60 g and 0.6 g of adsorbent dosage, respectively, at a pH 3 with a contact time of 170 min under room temperature. It was observed that the produced data fitted best with the pseudo-second order kinetic model and Freundlich isotherm model for characterising the adsorption of paracetamol onto OPF CNC hydrogel beads with a maximum adsorption capacity, q_{max} of 0.03 mg g^{-1} . Meanwhile, for OPF CNC-AC hydrogel beads, the pseudo-second order kinetic model and Langmuir isotherm model showed the best correlation for the adsorption of paracetamol with a q_{max} value of 21.31 mg g^{-1} . Therefore, the output from this study may suggest that OPF CNC and OPF CNC-

AC hydrogel beads can be used as natural adsorbents for the removal of paracetamol waste.

CHAPTER 1

INTRODUCTION

1.1 Background study

First and foremost, water is ultimately the essential compound on earth. This is due to the fact that it is required by all plants and animals. As a result of growing in population size and increased industrial enterprise, the demand for clean water has been increased (Mohammed et al., 2015). However, the development and the use of pharmaceutical compounds to treat human and veterinary diseases have rapidly increased, causing the water to be contaminated with organic compounds (Chen et al., 2013). A part of these compounds is excreted through faeces or urine from the body. In recent years, direct discharge such as pharmaceutical industry wastewater and indirect discharge like municipal and hospital effluents have become increasingly recognised emerging issues due to the harmful effects of pharmaceutical compounds on human and environmental health (Patel et al., 2019). Lei et al. (2015) point out that emerging pollutants are substances not protected by current water regulations but are considered a risk to ecosystems and human health.

Pharmaceuticals are natural or synthetic chemicals that can be used in prescription drugs, over-the-counter medicinal drugs, and veterinary medicines that contain active ingredients intended to have pharmacological effects and confer significant social benefits (Mukoko, 2016). Painkillers, anti-depressants, and birth control pills are examples of pharmaceutical products. Pharmaceutical compounds can navigate their way to wastewater collection systems that are ultimately discharged into wastewater facilities (Yan et al., 2014). As a result, residual amounts in treated water have accumulated in drinking water (Rivera-Utrilla et al., 2013). Some of the

pharmaceuticals are discharged into the surrounding after use, and some of them are disposed of as unused or expired products during manufacture (Bashaar et al., 2017). Non-target individuals and organisms can still be affected by the existence of pharmaceuticals in the watery environment even at relatively low doses (Coimbra et al., 2018).

Paracetamol is one of the pharmaceutical compounds found in natural water due to its widespread consumption. Paracetamol, also known as acetaminophen, is a non-steroidal anti-inflammatory medicine worldwide to relieve discomfort and reduce fever (De Laurentiis et al., 2014). This antipyretic medicine is easily and readily available even without a medical prescription. Thus, like the other pharmaceutical substances, the concentration of paracetamol may be significant in wastewater and water supplies (de Luna et al., 2013).

In order to prevent harmful effects on humans and the environment from polluted waters, effluents containing pharmaceutical compounds should be handled properly. Conventional wastewater treatment plants are typically designed to eliminate suspended solids, the need for biochemical oxygen demand (BOD), and pathogenesis. Therefore, they cannot eradicate medicinal substances effectively (Mashayekh-Salehi & Moussavi, 2016). Mashayekh-Salehi and Moussavi (2016) mentioned that adsorption is the most promising approach for eliminating pharmaceutical substances because of its high potential for adsorption, low energy cost, and environmental friendliness.

The evolution of another economical adsorbent derived from renewable substances has been motivated due to the high-priced and energy required in the manufacture and regeneration of the adsorbent (Mohammed et al., 2015). Recently,

there was a study of chitosan/biochar hydrogel beads on the adsorption of pharmaceutical contaminants such as paracetamol and ciprofloxacin (Afzal et al., 2018; Vakili, Amouzgar, et al., 2019). However, no comprehensive research reported on the hydrogel beads extracted from the oil palm biomass such as OPF for the adsorption of paracetamol.

The utilization of waste material from oil palm biomass as an economical adsorbent would be advantageous for both environmental and economic perspectives (Setiabudi et al., 2016). Maya et al. (2016) stated that lignocellulosic oil palm biomass is abundant with carbohydrates, and it consists of organic compounds such as cellulose, hemicelluloses, and lignin. A high-value by-product can be obtained from oil palm biomasses which can be used as sources of energy, fertilizers, animal food and furnishings, and paper manufacturing (Dungani et al., 2018). These biomasses represent a source of sustainable as well as renewable raw materials that approach the greener environment and are economically important. According to Haafiz, Hassan, et al. (2013), this situation approaches the manufacturing of green materials that draw the attention and curiosity of researchers to protect the environment. Finally, using environmentally friendly nanomaterials such as cellulose nanocrystals (CNC) to eliminate wastewater pollutants would significantly affect countries in the third world where water contamination has become a significant environmental problem.

1.2 Problem statement

Oil palm biomass is a lignocellulosic residue that contains cellulose, hemicellulose, and lignin. Malaysia has become the second-largest palm oil producer, and the biomass wastes have been increased regularly (Onoja et al., 2019). This biomass was generated in a large amount, but only a small fraction is used to make a

higher quality product. Therefore, to completely utilize this waste, the oil palm frond, one of the oil palm biomasses, will be used as a prospective raw material for the pre-treatment and extraction of cellulose nanocrystals.

Pharmaceutical waste discharged has become a significant concern (Department of Environment, 2019). Day by day, the pharmaceutical waste found in the wastewater has been increased. Paracetamol is one of the pharmaceutical compounds used worldwide, and it can bring adverse effects to humans. Thus, the presence of paracetamol in wastewater needs to be removed.

There is no comprehensive research report on the elimination of paracetamol using CNC hydrogel beads derived from oil palm fronds. Mostly, the activated carbon (AC) was reportedly used to remove the presence of paracetamol in an aqueous solution. However, activated carbon as the adsorbent material has been considered a high-cost adsorbent, requires a lot of energy, and its generation process is quite expensive (Setiabudi et al., 2016).

Therefore, the OPF CNC and OPF CNC-AC hydrogel beads could be utilized as the adsorbent for the adsorption of paracetamol as it has been revealed that CNC tends to be a good and natural adsorbent. Furthermore, they offer many advantages such as their more straightforward processing, significantly easier generation, the possibility of physical and chemical modification properties, the chance to shape them into sheets, beads and membranes, and the opportunity to control the pore structure and internal surface area *via* polymerization conditions (Coimbra et al., 2018).

1.3 Research objectives

The following objectives were focused on being accomplished in this study project:

1. To synthesize and characterize cellulose nanocrystals (CNC) extracted from oil palm fronds (OPF) using complementary analyses.
2. To produce and characterize the OPF CNC and OPF CNC-AC hydrogel beads using complementary analyses.
3. To determine the adsorption behaviour based on the effect of adsorbent dosage, pH, initial concentration, contact time, and reusability of the OPF CNC and OPF CNC-AC hydrogel beads for the removal of paracetamol.
4. To propose an adsorption mechanism based on spectroscopic analyses, adsorption isotherm, and kinetic studies.

1.4 Scope of study

This research involved characterisation of isolated OPF CNC using FTIR, CP/MAS ^{13}C NMR, XRD, TGA, DSC, BET, SEM, TEM, and OPF CNC hydrogel beads and OPF CNC-AC hydrogel beads using FTIR, BET, SEM, and EDX. Meanwhile, XPS analysis was carried out for only OPF CNC-AC hydrogel beads. The paracetamol adsorption studies on OPF CNC hydrogel beads were focused on adsorbent dosage (0.1 - 150 g), pH (1 - 11), initial concentration (1 – 1000 mg L⁻¹), and contact time (10 - 170 min), while OPF CNC-AC hydrogel beads focused on pH (1 - 11), initial concentration (1 – 1000 mg L⁻¹) and contact time (10 - 170 min). Adsorption isotherm models (Langmuir, Freundlich, Temkin, and Dubinin-Radushkevich) and adsorption kinetic models (pseudo-first order, pseudo-second order, Elovich model, and intra-particle diffusion) were used to determine the kinetics and equilibrium data.

CHAPTER 2

LITERATURE REVIEW

2.1 Oil palm (*Elaeis guineensis*)

Oil palm is one of Malaysia's most substantial commercial crops. The oil palm (*Elaeis guineensis*) is widely grown as a source of edible oil throughout West and Central Africa, as well as Malaysia, Indonesia, and Thailand (Barthel et al., 2018). Malaysia's world production was 27.7 %, while Indonesia's was 56.5 % in 2018 (Wardhani & Rahadian, 2021). Since mid-2006, Indonesia has overtaken Malaysia as the world-leading palm oil industry (Bentivoglio et al., 2018).

Malaysian Palm Oil Board (MPOB) indicated that approximately 5, 865, 297 ha of land was used as oil palm plantation area in 2020 (Table 2.1). Generally, the average perennial life period of the oil palm tree is 25 years old, accumulating measurements of about 45 - 65 cm in diameter and 7 - 12 m in height from the ground surface.

The industry of palm oil is among the essential agro-industries in Malaysia. It produces enormous amounts of solid oil palm waste in terms of oil palm leaves (OPL), oil palm trunks (OPT), oil palm fronds (OPF), empty fruit bunches (EFB), mesocarp fibres (MF), and palm kernel shells (PKS) (Setiabudi et al., 2016). This industry produced nearly 87 million tonnes of oil palm solid residue in 2020. The rapid growth of oil palm plantations has resulted in tremendous waste, complicating replanting activities and raising severe environmental issues. Around 4 kg of waste material is produced for every 1 kg of crude palm oil obtained (Sulaiman et al., 2011). Such solid wastes have no economic value and cause a significant issue in terms of disposal. Through the optimum utilization of oil palm biomass, all these problems can be

reduced, and these lignocellulosic materials can be used for great value-added products by biological, chemical, and physical developments.

Table 2. 1: Oil palm planted area by state in December 2020 (MPOB)

State	Total (ha)	Percentage yield (%)
Johor	740,828	12.6
Kedah	89,782	1.5
Kelantan	167,599	2.9
Melaka	56,361	1.0
Negeri Sembilan	190,462	3.2
Pahang	782,247	13.3
Perak	391,768	6.7
Perlis	694	0.0
Pulau Pinang	12,829	0.2
Selangor	126,525	2.2
Terengganu	178,628	3.0
Sabah	1,543,054	26.3
Sarawak	1,584,520	27.0
Malaysia	5,865,297	100.0

The abundance of oil palm waste, especially the oil palm fronds (OPF), has disposal problems that need to be handled. In the plantation area, oil palm fronds are usually leftover or burned. The fronds from harvesting and maintenance pruning were 43.3 million tonnes (Oviasogie et al., 2013). Currently, there is no primary commercial use for the fronds typically returned as mulching material to the soil. Investors have barely paid special attention to fronds and trunks even though they have a vast availability and possible commercial exploitation (Daud & Law, 2011). This may be partly because, in contrast with EFB, these biomasses are not explicitly involved in the process of palm oil milling. Furthermore, their commercial use would involve separate and distinct equipment for harvesting, transport, storage, and processing, creating extra capital costs.

Compared to other oil palm biomasses, OPF has a minuscule contribution to research work. The examples of other oil palm leftovers which have attracted the researchers' attention are OPL (Ahmad et al., 2018; Setiabudi et al., 2016), EFB (Tan et al., 2013; Thoe et al., 2019), OPT (Bukhari et al., 2020; Selamat et al., 2019), MF (Apriyanto et al., 2020; Chieng et al., 2017), and PKS (Gibigaye et al., 2019; Oti et al., 2017). To date, valuable products such as alternative energy sources (Abdullah et al., 2015; Kumneadklang et al., 2015), activated carbon (Lawal et al., 2020; Maulina et al., 2020), heavy metal adsorbent (Ehishan & Sapawe, 2018; Vakili et al., 2014), paper making material (Daud & Law, 2011; Jarupan et al., 2021), and green phenol substitutes (Hussin et al., 2013) has been successfully utilized from OPF.

2.2 Combinative pre-treatment process

Biomass pre-treatment is essential for extracting non-cellulosic materials and leaving only cellulosic components for subsequent nanocellulose extraction (Haafiz et al., 2014). According to Blanco et al. (2018), CNC is usually made by isolating cellulose before attacking it directly. Pre-treatment processes such as chemical, mechanical, biological, and combination techniques can be used to extract cellulose from lignocellulosic materials (Khalil et al., 2014). Besides, these processes are frequently utilized to make the hydrolysis process for CNC manufacturing easier. Several studies have recently utilized these pre-treatment techniques to remove non-cellulosic components from agricultural wastes.

Combinative pre-treatment of lignocellulosic biomass has received much interest because it guarantees increased efficiency, faster delignification, and less cellulose pulp severity (Timilsena et al., 2013). Generally, the combined pre-treatment procedure included hydrolysis of biomass and delignification process, respectively.

This method entails pre-soaking or pre-hydrolysis of biomass (as the first stage) to hydrolyse the hemicelluloses. Then, a delignification process (as the second step) is followed to retreat the product from the first step (Hussin, 2014). According to Baruah et al. (2018), the pre-hydrolysis process improved the extractability yield of cellulose by disrupting the lignin-carbohydrate bond and causing the crystalline structure of cellulose to be disrupted. Thus, resulting in the smaller lignin and cellulose fragments, as shown in Figure 2.1. These two-step processes' primary purpose is to disrupt the cellulose fibres in the biomass by breaking the lignin seals.

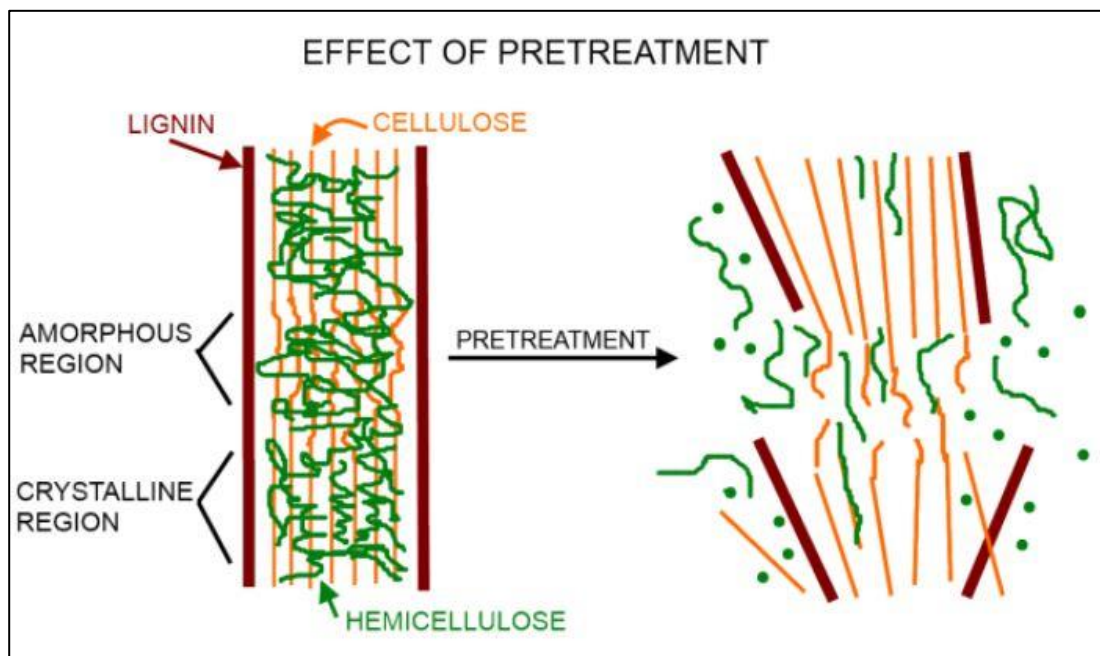


Figure 2. 1: Schematic diagram of pre-treatment on lignocellulosic biomass (Muley & Boldor, 2017)

2.2.1 Autohydrolysis

Autohydrolysis or hydrothermal is a type of pre-treatment known to be ecologically benign because the reaction is solely based on water. This method is performed to eliminate the unwanted hemicellulose component, leaving just the required cellulose component. Some earlier studies have shown that autohydrolysis

enhances the characteristics of pre-treated biomass with high porosity and specific surface area while leaving a small amount of residue (Liu et al., 2019).

As displayed in Figure 2.2, the autohydrolysis process involves heating lignocellulosic biomass to a high temperature and pressure, which causes acid components to dissolve, ester groups to de-esterify, and organic acids to form in the hemicellulose structure (Samuel et al., 2013).

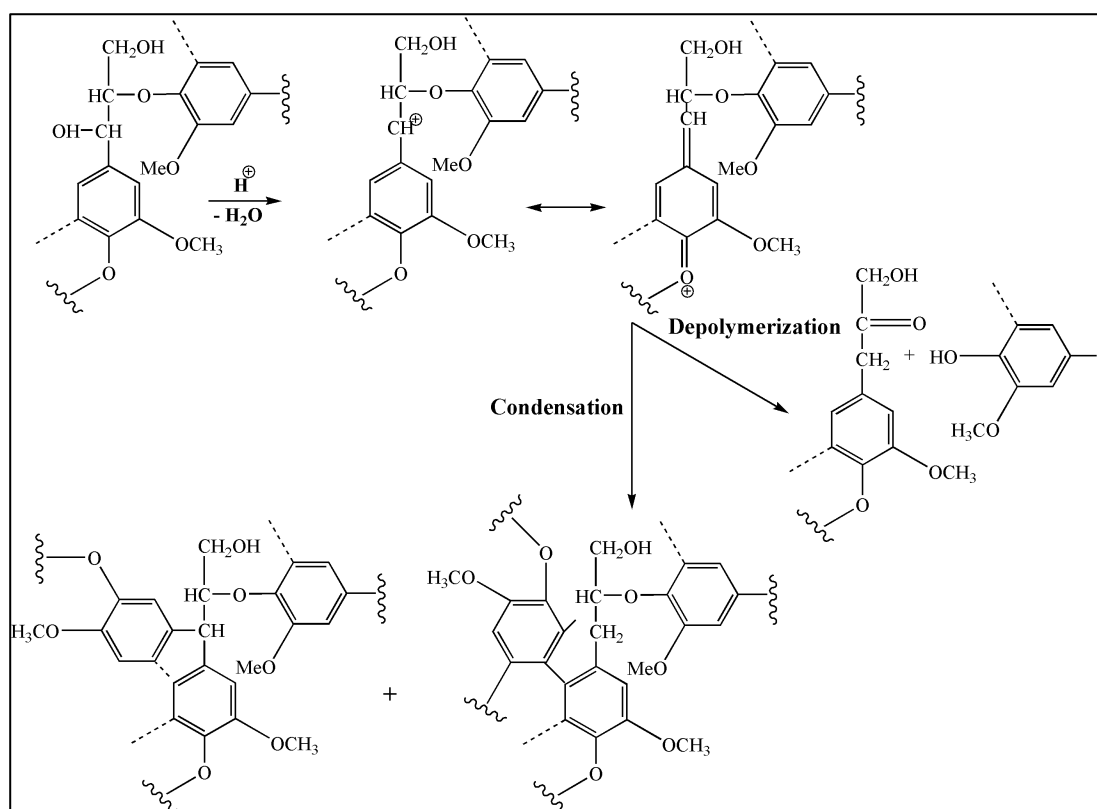


Figure 2. 2: A possible mechanism during autohydrolysis process

The acetyl groups in biomass are cleaved, resulting in organic acid (such as acetic acid) and causing hemicellulose hydrolysis, which occurs spontaneously (Tan et al., 2018). Apparently, due to the mechanistic effect of hydronium ions on lignocellulosic materials, the autohydrolysis treatment would particularly break down the hemicellulose part, which could then be recovered in the residual solution (Walch et al., 1992). According to Timilsena (2012) as cited by Tan et al. (2018), the liquid

portion, which is high in hemicellulose, could be used to make furfural derivatives or other green chemicals. Removing hemicellulose from lignocellulosic biomass would improve cellulose hydrolysability, producing a solid pulp high in cellulose and insoluble excess lignin (Garrote et al., 1999). In addition, to assure the efficacy of the delignification capability of treated biomass, it is necessary to optimize the operating parameters during autohydrolysis. For example, the elimination of hemicellulose, delignification yield, and the conversion effectiveness of cellulose to glucose throughout enzymatic hydrolysis have all been affected by the operating conditions of *Miscanthus x giganteus* biomass during autohydrolysis (Tan et al., 2018).

2.2.2 Delignification process

The use of alkaline to remove the amorphous polymer of hemicellulose and the residual lignin is known as an alkaline treatment (Phanthong et al., 2018). Several chemical agents are employed in this chemical pulping process to break down lignin and hemicellulose surrounding the cellulose fibres (Trache et al., 2017). Hussin et al. (2013) reported that different forms of delignification processes, including Kraft pulping, soda pulping, and organosolv pulping, are thought to significantly impact lignin's extraction yield, structure, and physicochemical properties. The ether and ether linkage of the larger structure of lignin would be broken during this process. Subsequently, the resulting fragments are dissolved in the solution and produced a black liquor (Tan et al., 2018).

2.2.2(a) Soda pulping

Soda pulping refers to a chemical pulping process using sodium hydroxide (NaOH) as a delignification agent to dissolve lignin from biomass. It was first developed in England in 1851 (Holm, 2018). Soda pulping is gaining popularity due

to the biorefinery concept that has enhanced interest in sulphur-free lignin and nanocrystalline cellulose. According to Gomes et al. (2014), a sulphur-free approach reduces sulphur emissions in the atmosphere and eliminates the need for additional desulphurization stages. The creation of minor quantities of phenolic hydroxyls and the degradation of primary aliphatic –OH occur during soda pulping, resulting in the breakage of aryl-ether bonds (Figure 2.3) (Hussin, 2014). Since cellulose and lignin are destroyed concurrently during the pulping process, the soda pulping procedure generates pulp with poor tearing strength. Besides, using anthraquinone (AQ) as an additive throughout this method to improve lignin's output has been recommended to reduce cellulose degradation (Hussin, 2014).

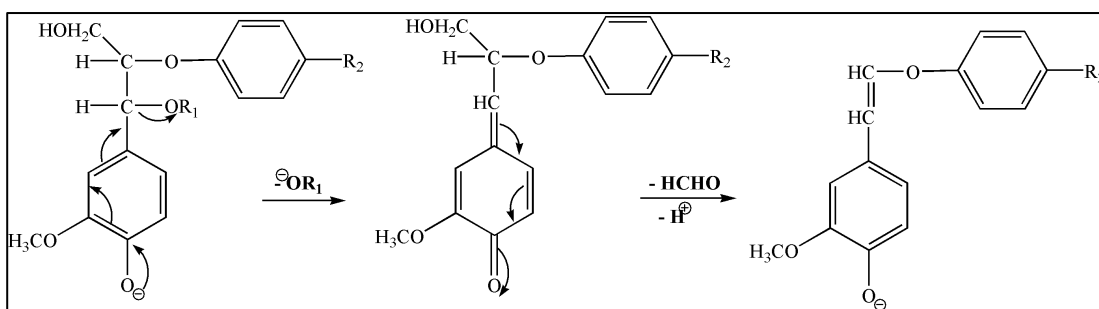


Figure 2. 3: Mechanism of lignin during soda pulping process

In terms of process structure, soda pulping is quite comparable to Kraft pulping, making it an appealing process alternative. Soda lignin is recovered in the same way Kraft lignin is by precipitating black liquor with mineral acids.

2.3 Chemical techniques for CNC isolation

According to Trache et al. (2017) and Xie et al. (2018), the production of nanocellulose from cellulose usually involves two steps. The first step is pre-treatment of lignocellulosic biomass to acquire pure cellulose, while the second step is converting cellulose into nanocellulose. The second step guarantees that the

amorphous domains from pure cellulose are removed, resulting in CNC formation (Dufresne, 2017; Jonoobi et al., 2015). Improved chemical acid hydrolysis (Kontturi et al., 2016), mechanical treatment (Pandey et al., 2013), oxidation process (Sun et al., 2015), ionic liquid treatments (Lazko et al., 2016), subcritical water hydrolysis (Novo et al., 2016), enzymatic hydrolysis (Tong et al., 2020), deep eutectic solvents (Sirviö et al., 2016), and combination processes (Trache et al., 2017; Trache et al., 2020) have all been reported as approaches for obtaining CNC.

The mechanical treatment method has been extensively researched for the generation of nanocellulose, whether as part of the fabrication process employing a mix of acid hydrolytic, oxidative, and enzymatic treatment or as a stand-alone method (Amin et al., 2015). Micro fluidization, ultrasonication, high-pressure homogenization, and ball milling are examples of mechanical treatment. Amin et al. (2015) have recently devised a scalable mechanical approach based on high-energy bead milling. CNC was extracted from commercial microcrystalline cellulose (MCC) micronized by high energy bead milling and aqueous dispersion. They discovered that the CNC structure and aspect ratio values were like the acid hydrolysis method with a 57 – 76 % yield.

Saito and Isogai (2006), as cited by Trache et al. (2017) published a paper that described a new approach for introducing charged carboxylate groups into cellulosic materials. This method assisted disintegration into nanofibers with smaller diameters while requiring far less energy than the standard mechanical treatment. Trache et al. (2017) reported that the oxidation method takes place in amorphous domains and on the cellulose fibres' surface. When the carboxyl content of cellulose reaches a particular level, it begins to scatter in an aqueous medium. However, the crystalline domains remain undamaged and can thus be freed (Dufresne, 2017). Researchers used

a direct ultrasonic-assisted TEMPO–NaBr–NaClO technique to make carboxylic cellulose nanocrystals from the pulp of cotton linter. This technique has been used by Cao et al. (2012). They could produce a transparent and efficient translucent dispersion of CNC (80% yield).

Only a few studies have been published on CNC manufacturing using subcritical water hydrolysis (Novo et al., 2015; Novo et al., 2016). The use of water exclusively as a reagent is a good process because of its environmental benefits and the low and cleaner effluent, minimal corrosion, and low reagent cost. Using the subcritical water hydrolysis method, Novo et al. (2015) produced CNC using commercial microcrystalline cellulose. According to the authors, optimizing process parameters leads to a high-quality CNC with a greater yield.

Besides, scientists are becoming interested in ionic liquids. This is because it is reusable, durable, has low melting temperature and low vapor pressure reagents, contributing to novel and sustainable solutions (Trache et al., 2017). They have exceptional solvating capabilities and are developing as eco-friendly solvents to pre-treatment and process lignocellulosic materials. Ionic liquids' reusability seems necessary for conceptualizing any environmentally and economically effective CNC isolation technique. Furthermore, ionic liquids are an effective alternative reaction media for selective and controlled cellulose hydrolysis, resulting in the extraction of nanoscale particles in several recent investigations (Trache et al., 2017).

2.3.1 Acid hydrolysis

An acid hydrolysis process has been widely investigated in order to extract nanofibers from various cellulosic biomass. It is stated that hydrolytic conditions have a major impact on the surface charge and size of the nanocellulose fibres. The

hydrolytic conditions are temperature, acid-to pulp ratio, response time, and form of acid.

Acid hydrolysis is a process in which disordered, or para-crystalline portions are initially solubilized, leaving behind the acid-resistant crystalline regions or CNC (Phanthong et al., 2018). The schematic diagram of CNC separation in acid treatment can be seen in Figure 2.4. Acid hydrolysis will break the hydrogen bonds and splits the fibre's amorphous regions, resulting in transparent crystalline rods. In this process, sulphuric acid (H_2SO_4) and hydrochloric acid (HCl) is usually used to extract the amorphous regions for CNC production (Trache et al., 2017). Other acids that can be employed in acid hydrolysis include phosphoric acid and hydrobromic acid, but the most frequently used are sulphuric and hydrochloric acids. Different types of acid utilized for the acid hydrolysis process to form cellulose derivatives from various cellulosic biomass and their crystallinity index value are listed in Table 2.2.

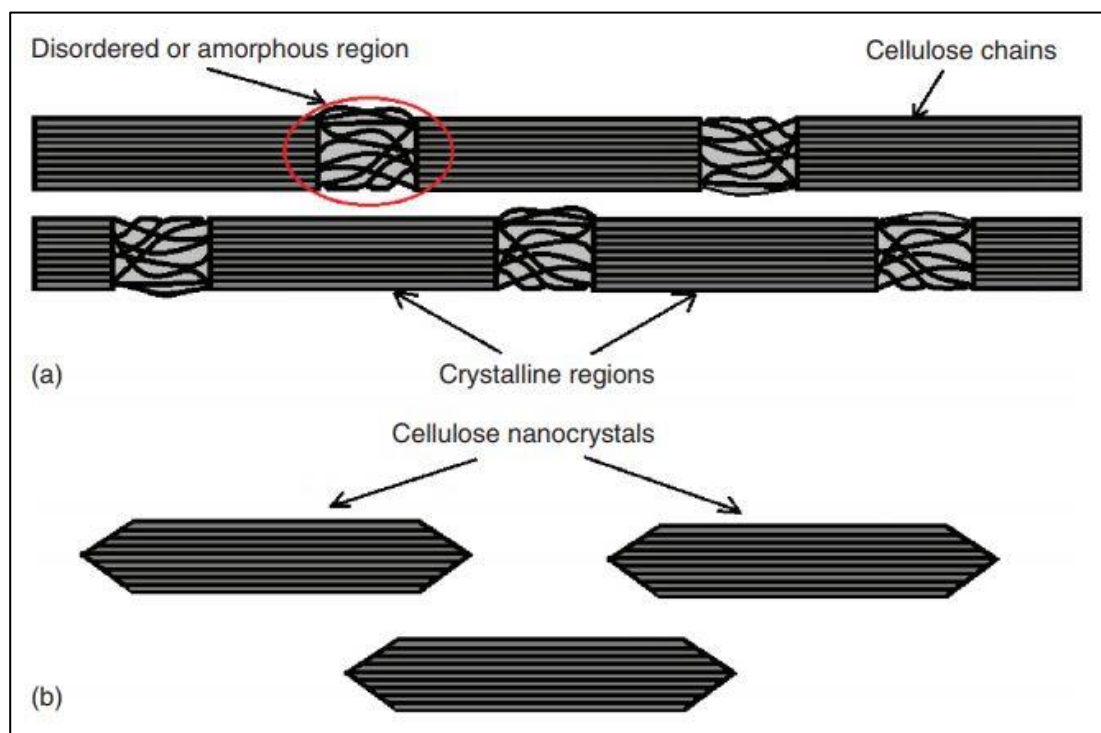


Figure 2. 4: (a) Schematic diagram of the amorphous and crystalline regions in cellulose break down during acid hydrolysis and (b) isolated CNC (Moon et al., 2011)

CNC produced particular functional groups on the surface of the nanoparticles by using several acid treatments, each of which impacts their colloidal stability (Grishkewich et al., 2017). The dispersibility of CNC derived from these acids also is dissimilar. Due to the numerous charged sulphate or phosphate groups on its surface, CNC formed from sulphuric or phosphoric acid hydrolysis is easily dispersed in the water. However, those CNC produced from hydrochloric and hydrobromic acid hydrolysis are difficult to disseminate as their aqueous suspensions seem to flocculate (Blanco et al., 2018). According to Lu et al. (2013), sulphuric acid hydrolysis is a typical process for producing cellulose nanofibers since the technique can disintegrate amorphous regions, applying negative charges to surfaces of nanoparticles and creating stable suspensions of nanocrystals. Furthermore, CNC formed from hydrochloric acid hydrolysis shows low colloidal stability, while CNC obtained from sulphuric acid has negatively charged groups of sulphate esters on its surface, stimulating repulsive forces to produce an extremely stable colloidal dispersion. In addition, with the inclusion of sulphate groups on the surface of crystallites, sulphuric acid gives a very stable aqueous suspension (Jonoobi et al., 2015).

Table 2. 2: Different types of acid used to form cellulose derivatives from various kinds of sources and their crystallinity index

Source	Process	Crystallinity index (%)	References
Kenaf	H ₂ SO ₄ hydrolysis	70.0	(Hussin et al., 2019)
Filter paper	H ₂ SO ₄ hydrolysis	78.0	(Li et al., 2019)
Poplar chips	H ₂ SO ₄ hydrolysis	–	(Ma et al., 2019)
Cotton fabric	H ₂ SO ₄ hydrolysis	–	(Song et al., 2017)
Corncob	H ₂ SO ₄ hydrolysis	57.7	(F. Yu et al., 2016)
Aspen pulp	H ₂ SO ₄ hydrolysis	63.0	(Jin et al., 2015)
Sludge	H ₂ SO ₄ hydrolysis	–	(Z. Karim et al., 2014)
Groundnut shell	HCl hydrolysis	–	(Zango & Imam, 2018)
Dried rice bran	HCl hydrolysis	67.0	(Arowona et al., 2018)
Cotton wool	HCl hydrolysis	–	(Arowona et al., 2018)

Note: “–” specifies the relevant information was not stated in the reference.

2.3.1(a) Cellulose hydrolytic mechanism in acid hydrolysis

The mechanism is a crucial reaction process that explains how chemical substances turn into other ones. Some bonds are broken, and new ones are generated during the transformation. According to Joksimović and Marković (2007), strong mineral acids are found to hydrolyse cellulose more efficiently than weak acids. For example, sulphuric acid hydrolyses almost all cellobiose, while only 80% of the glucose is produced.

The β -1, 4-glycosidic linkages of a cellulose chain molecule are broken by water molecules when cellulose is hydrolysed in an acidic media to glucose. This addition gives fragments of shorter chain lengths while keeping the basic structure (Fan et al., 1987). The H⁺ ions from the acid solution will travel to the β -glycosidic linkage in cellulose, whereas SO₄²⁻ ions will reduce the strength of the bond and speed up the hydrolysis process. Therefore, the glycosidic bond will dissolve, and the

cellulose H-bonded structure will begin to open. In addition, hydronium ion (H_3O^+) is generated by protonation from the acid solution throughout glucose degradation and cellulose hydrolysis (Tan et al., 2018).

According to Lelekakis et al. (2014), the reaction of cellulose hydrolysis followed by glucose degradation has been represented as a pseudo-first order sequential homogeneous reaction concerning the concentration of H_3O^+ . Historically, Saeman (1945) has conducted the first comprehensive study on the kinetics of cellulose hydrolysis to glucose. Acid hydrolysis of cellulose produces free glucose molecules, which are then degraded into hydroxymethylfurfural (a furan), levulinic acid, formic acid, and other acids by further acid hydrolysis, as shown in Figure 2.5 (Lelekakis et al., 2014).

The mechanism of cellulose hydrolysis is thought to be like that of acid-catalysed glycoside hydrolysis. The protonation of glycosidic oxygen (pathway I) or pyranic oxygen (pathway II) is the first step in this acid hydrolysis mechanism, as shown in Figure 2.6 (Rinaldi & Schüth, 2009). In theory, considering the H_3O^+ nature and the conformational restriction of cellulose chains along with the glycosidic bond, both oxygen atoms should be partially protonated. The production of the carbocation *via* a unimolecular step is a critical stage in the mechanism as it is thought to produce either a cyclic (pathway I) or an acyclic (pathway II) carbocation (Tan et al., 2018).

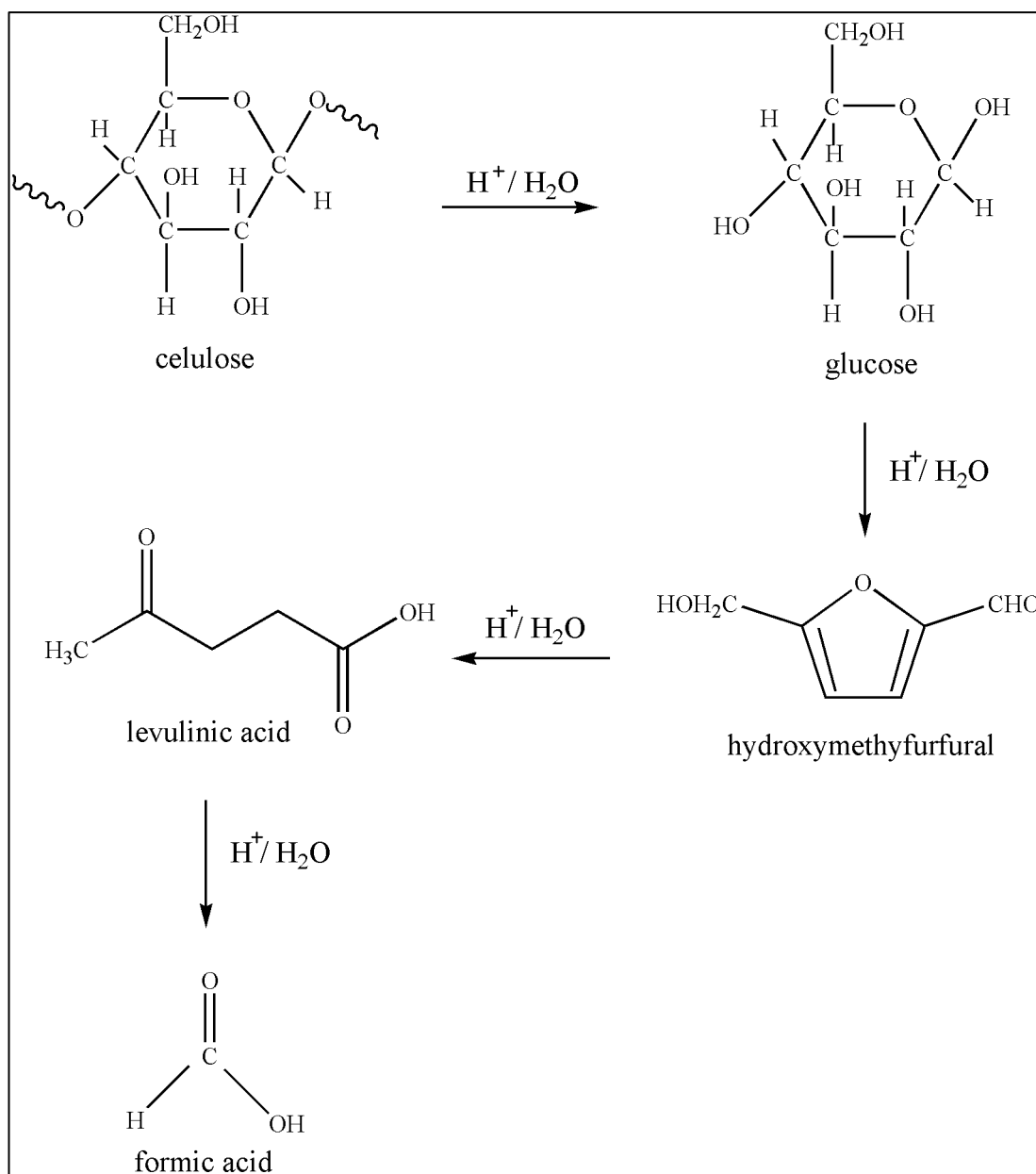


Figure 2. 5: The acid formation in cellulose

Edward (1955) proposed, as cited by Rinaldi and Schüth (2009), that the reaction proceeds *via* a cyclic carbocation due to the stability of methyl glycosides against acid hydrolysis. The hydrogen and hydroxyl groups are omitted for clarity. The tetrahydropyran ring goes through a ring flipping to a half-chair conformation required to create this cyclic intermediate. Due to the rotational constraints generated by intermolecular and intramolecular H-bonding in the supramolecular cellulose structure, the second step in pathway I is anticipated to be energetically demanding

(Rinaldi & Schüth, 2009). These constraints are relaxed in homogeneous cellulose hydrolysis, resulting in several orders of magnitude higher hydrolysis rates than those seen in heterogeneous hydrolysis. Meanwhile, water reacts with the carbocation in the third step, re-establishing the anomeric centre and regenerating the H_3O^+ species. Rinaldi and Schüth (2009) reported that the molecular process of cellulose hydrolysis is based on similar disaccharide reactions, implying that cellulose is hydrolysed *via* pathway I. Nevertheless, alternate pathway II can be suggested, but it is unclear whether it is essential in cellulose hydrolysis as further investigations are still required (Tan et al., 2018).

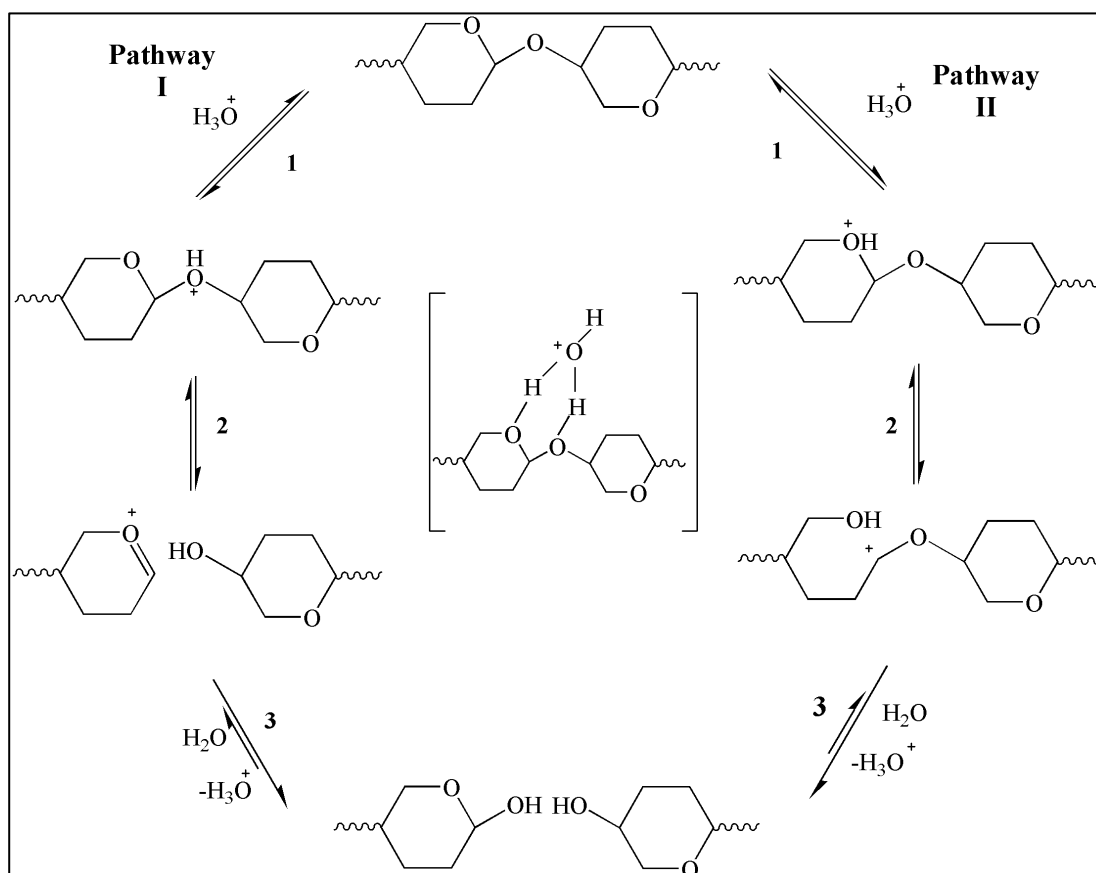


Figure 2. 6: Mechanism of acid hydrolysis of glycosidic bonds

2.4 Cellulose

Cellulose (Figure 2.7) is the world's most extensive organic biopolymer material and is present in plants, animals, and other microorganism cells as the primary structural part. It is estimated that cellulose production around the world is over 7.5×10^{10} tonnes per year (Khalil et al., 2014). In most plant cell walls, cellulose, a ubiquitous organic compound, is considered the essential basic component structure relating to their excellent stability and strength capabilities. Based on the origin of cellulose, the cell wall components in plants have a strengthening function, and their structure can differ significantly (Daras et al., 2021). For a variety of reasons, the quantity of cellulose in fibre has an impact on its use, development, and quality. Cellulose as a feedstock for functionalized materials has caught great interest in the chemistry community for over a century because cellulose is the most plentiful sustainable polymer in the world (Tu et al., 2021).

Carbon (44.44 %), hydrogen (6.17 %), and oxygen (49.39 %) are the main constituents of cellulose (Blanco et al., 2018). $(C_6H_{10}O_5)_n$ is the chemical formula of cellulose, where n stands for the degree of polymerization (DP) and indicates the number of glucose units (Blanco et al., 2018). The cellulose's degree of polymerization varies depending on the cellulose fibre's source and handling technique.

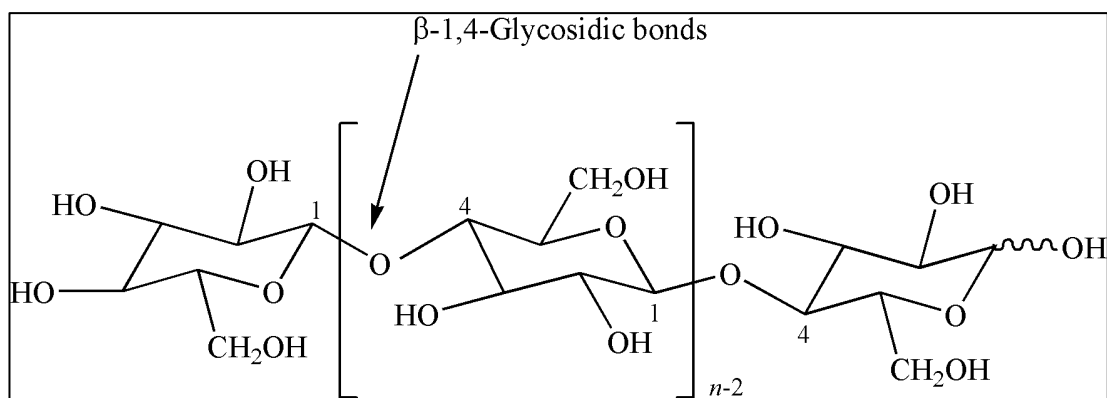


Figure 2. 7: Molecular structure of cellulose chain where n is the value of a degree of polymerization

Chemically, the cellulose structure constructs D-anhydroglucose ($C_6H_{11}O_5$) units from a linear polymer made up of cellulose monomers, which are connected by β -(1-4) glycosidic linkages to generate dimer cellobiose, which are the repeating units of the cellulose chain (Phanthong et al., 2018). This cellulose chain is long, straight, and nearly fully stretched. The cellulose is rotated 180° relative to each other along the central axis. By generating intramolecular and intermolecular hydrogen bonds between OH groups in the same cellulose chain and the surrounding cellulose chains, the chains are likely to be ordered in parallel and create a crystalline supramolecular structure (Trache et al., 2017).

The long chain of cellulose is referred to as alpha-cellulose, where the β -1, 4 glucan chain depends on the source of the cellulose (Trache et al., 2017). Cellulose from glucose molecules ($C_6H_{12}O_6$) is a monosaccharide formed from carbon dioxide *via* the photosynthesis process. The three free hydroxyl groups located at C6 (primary hydroxyl groups), C2 and C3 (secondary hydroxyl groups) are organized into intramolecular and intermolecular hydrogen bonds in glucose units (Phanthong et al., 2018). These two hydrogen bonds are linked to produce highly organised 3-D

crystalline structures that support the network, supplying a plant with strength, rigidity, and structural stability.

There are four different polymorphs in cellulose: celluloses I, II, III, and IV (Hussin et al., 2016). Cellulose I, also called native cellulose, is a thermodynamically meta-stable structure. It exists naturally and can be converted to celluloses II, III, or IV. Cellulose I occurs naturally in two crystalline sub-allomorphs, cellulose I- α (a cell structure of the triclinic unit) and cellulose I- β (a cell structure of the monoclinic unit), both of which are found predominantly in plant species. The origin of cellulose affected the proportion of both crystalline forms (Blanco et al., 2018). For example, bacterial cellulose is abundant with cellulose I α while cellulose I β is relatively rich in the superior plant cell wall. The hydrogen bond and chain patterns differentiate the crystalline structure of cellulose I from that of regenerated cellulose II (Sehaqui et al., 2012). Cellulose II is infrequently found in the environment, and it can be synthesized or mercerized from cellulose I (Hussin et al., 2016). Cellulose II is the most thermodynamically stable crystalline form that results from recrystallization or mercerization of aqueous sodium hydroxide (Negahdar et al., 2016). In cellulose II, O3-H-O5 is the dominant intra-chain hydrogen bond, making the cellulose chain rigid and linear in shape. The only difference between cellulose I and cellulose II appear to be that cellulose II has an anti-parallel packing, and O6-H-O2 is the inter-chain bond (Figure 2.8) (Phanthong et al., 2018).

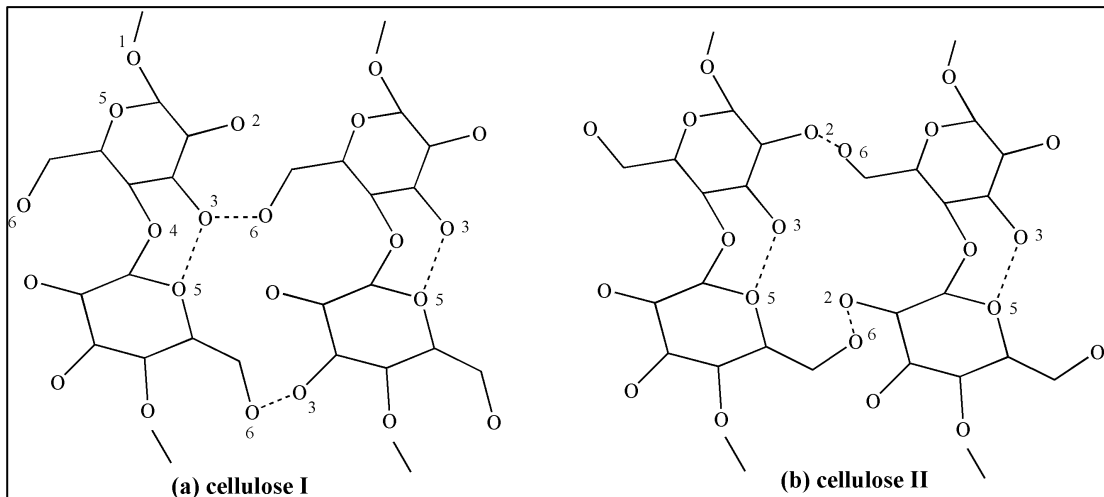


Figure 2. 8: Structure of cellulose I (a) and cellulose II (b)

In addition to these structures, more cellulose allomorphs are known: cellulose III and cellulose IV. Additionally, cellulose III will be generated by treating cellulose I with liquid ammonia followed by washing with alcohol. However, cellulose IV is produced in an acceptable liquid under pressure at high temperature while the other modified cellulose is processed (Klemm et al., 2019).

Cellulose is also generally known as fibrillar, crystalline, showing its different structural hierarchy of numerous biological origins (Lu et al., 2013). It is commonly used due to its outstanding properties such as availability, biocompatibility, biological degradability, sustainability, excellent reinforcing capacity, thermal stability, and environmental benefits. Due to the growing demand for green biocompatible materials, cellulose is thought to be an almost inexhaustible raw material source (Gan et al., 2020). Moreover, cellulose fibres have generally low elasticity and relatively high density compared to synthetic fibres and more vital electricity and heat conductors. It can still quickly form water-soluble sugars through acid hydrolysis. Cellulose chemical modification is a promising method to modify its physical and